American Mineralogist, Volume 92, pages 1112–1118, 2007

High-pressure phase relations and crystal chemistry of calcium ferrite-type solid solutions in the system $MgAl_2O_4$-Mg_2SiO_4

Hiroshi Kojitani,* Ryosuke Hisatomi, and Masaki Akaogi

Department of Chemistry, Faculty of Science, Gakushuin University, 1-5-1 Mejiro, Toshima-ku, Tokyo 171-8588, Japan

Abstract

To map the stability field of calcium ferrite-type $MgAl_2O_4$–Mg_2SiO_4 solid solutions, high-pressure phase relations in the system $MgAl_2O_4$-Mg_2SiO_4 were studied in the compositional range of 0 to 50 mol% Mg_2SiO_4. The calcium ferrite solid solutions are stable above 23 GPa at 1600 °C, and the maximum solubility of Mg_2SiO_4 component in $MgAl_2O_4$ calcium ferrite is 34 mol%. Lattice parameters and unit-cell volume of calcium ferrite-type $MgAl_2O_4$ (space group *Pbnm*) determined by Rietveld analysis are $a = 9.9498(6)$ Å, $b = 8.6468(6)$ Å, $c = 2.7901(2)$ Å, and $V = 240.02(2)$ Å^3. Lattice parameters for the $MgAl_2O_4$–Mg_2SiO_4 solid solutions with the compositions of 14, 24, and 34 mol% Mg_2SiO_4 indicated the following compositional dependency of lattice parameters: a (Å) = $9.9498 + 0.1947 \cdot X_{Mg_2SiO_4}$, b (Å) = $8.6468 - 0.1097 \cdot X_{Mg_2SiO_4}$, and c (Å) = $2.7901 + 0.0086 \cdot X_{Mg_2SiO_4}$, where $X_{Mg_2SiO_4}$ is the mole fraction of Mg_2SiO_4 component. A linear extrapolation of the composition-molar volume relationship gave an estimated volume of 36.49(2) cm^3/mol for the hypothetical calcium ferrite-type Mg_2SiO_4. This value is larger than that of the isochemical mixture of $MgSiO_3$ perovskite and MgO, 35.72(1) cm^3/mol. This implies that the mixture of $MgSiO_3$ perovskite and MgO is more stable than the hypothetical calcium ferrite-type Mg_2SiO_4 under the lower mantle conditions.

Keywords: $MgAl_2O_4$, Mg_2SiO_4, calcium ferrite, high pressure, phase relation, Rietveld refinement

Introduction

$MgAl_2O_4$ spinel is an important mineral in the Earth's upper mantle. The spinel decomposes to MgO periclase + Al_2O_3 corundum at about 15 GPa (e.g., Akaogi et al. 1999). Irifune et al. (1991) first reported that the oxide mixture reacts to form a phase with the calcium ferrite-type structure at about 25 GPa. Because the calcium ferrite structure has tunnel-like large cation sites suitable for alkali ions, it has been proposed as a possible structure for a high-pressure AB_2O_4 compound that could host alkali elements in the Earth's deep mantle (e.g., Ringwood et al. 1967). Recent high-pressure and high temperature experiments of mid-oceanic ridge basalt (MORB) considering subducted oceanic crust into deep mantle showed existence of aluminous phases with the calcium ferrite-type structure at lower mantle conditions (Kesson et al. 1994; Hirose et al. 1999; Funamori et al. 2000; Ono et al. 2001a, 2002). Chemical analyses of these phases indicated that they consisted mainly of $NaAlSiO_4$ and $MgAl_2O_4$ components. Guignot and Andrault (2004) noticed that the calcium ferrite phase in the high-pressure phase assemblage of MORB also contained a relatively large amount of Mg_2SiO_4 component. In general, it is convenient to treat the calcium ferrite phase as a solid solution among $MgAl_2O_4$, $NaAlSiO_4$, Mg_2SiO_4, and other minor end-members. However, detailed information of the calcium ferrite solid solutions is limited to the $MgAl_2O_4$-$CaAl_2O_4$ system (Akaogi et al. 1999).

Considering the coupled substitution, $2Al^{3+} = Mg^{2+} + Si^{4+}$, which has been observed in various solid solutions such as majorite garnet solid solution in the system $Mg_3Al_2Si_3O_{12}$-$Mg_4Si_4O_{12}$, it is likely that the same substitution occurs in $MgAl_2O_4$ calcium ferrite, resulting in a solid solution between $MgAl_2O_4$ and Mg_2SiO_4. Therefore, it is interesting from crystal chemical and geochemical points of view to determine how much Mg_2SiO_4 component can be incorporated into $MgAl_2O_4$ calcium ferrite.

In this study, the stability field of the calcium ferrite phase in the $MgAl_2O_4$-Mg_2SiO_4 system was established at pressures up to 27 GPa. The maximum solubility of Mg_2SiO_4 component was of particular interest. Only lattice parameters at ambient and high pressure have been determined for the calcium ferrite-type $MgAl_2O_4$ (Irifune et al. 1991, 2002; Yutani et al. 1997; Funamori et al. 1998). In this study, the structure was refined using the Rietveld method to determine the atomic positions and displacement parameters. Lattice parameters of some members of $MgAl_2O_4$–Mg_2SiO_4 solid solution were also determined to establish changes in the lattice parameters as a function of composition. Instability of the hypothetical calcium ferrite-type Mg_2SiO_4 is also discussed using its volume estimated by extrapolation from those of the known solid-solution members.

Experimental methods

High-pressure phase relations

High-pressure phase relation experiments in the system $MgAl_2O_4$-Mg_2SiO_4 were done with a Kawai-type multi-anvil high-pressure apparatus at Gakushuin University. The truncated edge length of tungsten carbide anvils was 1.5 mm. The pressure medium was a semi-sintered MgO octahedron. A cylindrical Re heater was put into the pressure medium together with a $LaCrO_3$ sleeve for thermal insulation. The powder sample was placed directly in the Re heater. Temperature was measured with a Pt/Pt-13% Rh thermocouple whose hot junction was positioned in the central part of the heater. Pressure was calibrated at room temperature using

* E-mail: hiroshi.kojitani@gakushuin.ac.jp

0003-004X/07/0007–1112$05.00/DOI: 10.2138/am.2007.2255

semiconductor-metal transitions of ZnS (15.5 GPa), GaAs (18.3 GPa), and GaP (23 GPa). The pressure was further calibrated at 1600 °C using the α-β transition of Mg_2SiO_4 at 15 GPa (Morishima et al. 1994) and the ilmenite-perovskite transition of $MgSiO_3$ at 23 GPa (Ito and Takahashi 1989; Ono et al. 2001b). More details on the high-pressure techniques used in this study can be found in Suzuki and Akaogi (1995) and Kubo and Akaogi (2000). Starting materials were mixtures of reagent grade MgO, Al_2O_3, and SiO_2 (silicic acid) with $MgAl_2O_4$ to Mg_2SiO_4 mole ratios of 90:10, 78:22, 70:30, and 50:50. These oxide powders were mixed in an agate mortar under ethanol and then heated at 1000 °C for 3 h to remove water in the silicic acid. The starting materials were held at 1600 °C and 21–27 GPa for 3 h and then quenched to room temperature while under pressure. After quenching, the pressure was released, and the samples were recovered. Phase identification was made using a micro-focused X-ray diffractometer (Rigaku RINT2500V, Cr*K*α, 45 kV, 250 mA) whose beam was collimated to a 50 μm spot in diameter. A scanning electron microscope (JEOL JSM-6360) with energy dispersive spectrometer (Oxford INCA x-sight) (SEM-EDS) was used to analyze the phase compositions in the center part of the recovered samples. Acceleration voltage and probe current were 15 kV and 0.35 nA, respectively. Standards for chemical analysis were synthetic Al_2O_3 corundum for aluminum and synthetic $MgSiO_3$ orthoenstatite for magnesium and silicon.

Rietveld refinement and lattice parameter determination of calcium ferrite solid solutions

Calcium ferrite-type $MgAl_2O_4$–Mg_2SiO_4 solid-solution samples used for the lattice parameter determinations were synthesized by the same method as for the above high-pressure phase relation experiments. Pure $MgAl_2O_4$ calcium ferrite was synthesized by holding the synthetic $MgAl_2O_4$ spinel at 27 GPa and 2200 °C for 1 h. The temperature above 1800 °C was estimated by extrapolating an electric power-temperature relationship. In syntheses of calcium ferrite-type $MgAl_2O_4$–Mg_2SiO_4 solid solutions, starting materials were the same oxide mixtures as used for the phase relation experiments, and were held at 27 GPa and 1800 °C for 3 h. To prepare specimens for XRD analysis, the synthesized polycrystalline samples were crushed into grains ~50 μm in size using a tungsten carbide die at the liquid nitrogen temperature. This cold manipulation prevented potential amorphization or retrogressive transition during crushing.

Powder XRD profiles were collected using a Rigaku RINT 2500V diffractometer. Data collection was made in the 2θ range 20–140° with a step size of 0.02° and counting time of 26 s per step. Rietveld analysis was done with the RIETAN-2000 program (Izumi and Ikeda 2000). When phases other than calcium ferrite, i.e., corundum or perovskite, were observed in an XRD profile, these phases were included in the Rietveld analysis. In the analysis of the solid solutions, isotropic displacement factors were fixed at those determined for pure $MgAl_2O_4$ calcium ferrite, and site occupancies of both Mg^{2+} and Si^{4+} in two different Al sites were assumed to be equal.

Raman spectroscopy

The calcium ferrite-type $MgAl_2O_4$ sample was the same as that used in Kojitani et al. (2003), and the $MgAl_2O_4$–Mg_2SiO_4 solid-solution samples were the run product of the high-pressure phase relation experiments in this study. All of them were well polished on the surface. The measurements were performed using a micro-Raman spectrometer (JASCO NRS-3100) at Gakushuin University. The wavelength and beam diameter of the laser were 532 nm and 1 μm, respectively. Laser power at the sample surface was approximately 5 mW. Slit width was 0.1 mm. Raman data were collected by repeated exposures of 50 s five times with a data interval of 0.05 cm^{-1}. The Raman shifts were calibrated with a Ne lamp. Raman peaks were analyzed using the software PeakFit (SPSS Inc.).

Results and discussion

High-pressure phase relations

Results of the phase transition experiments in the $MgAl_2O_4$-Mg_2SiO_4 system at 1600 °C are summarized in Table 1, and the derived phase relations are shown in Figure 1. Compositions of observed phases are tabulated in Table 2. The coexistence of garnet and calcium ferrite in all of the samples at 23 GPa and 1600 °C suggests that there is a phase boundary between (corundum + periclase + garnet) and (corundum + periclase + calcium ferrite or garnet + periclase + calcium ferrite) at about 23 GPa. In particular, a trace amount of garnet was observed in run no. 3. This indicated that a triple point among three different assemblages [(corundum + periclase), (calcium ferrite + corundum + periclase), and (garnet + corundum + periclase)] is at the composition of 10 mol% Mg_2SiO_4. Compositions of the corundum phases in the other runs at 23 GPa (runs no. 6, no. 11, and no. 14) contain ~10 mol% $MgSiO_3$ component. No garnet was observed in run no. 1 at 21 GPa and run no. 2 at 22 GPa, which had the same starting composition as that of run no. 3. The corundum from run no. 10 at 21 GPa also contained ~10

Table 1. Results of high-pressure experiments in the system $MgAl_2O_4$-Mg_2SiO_4

Run no.	Starting composition $MgAl_2O_4$:Mg_2SiO_4 (mole ratio)	Pressure (GPa)	Temperature (°C)	Run products
1	90:10	21	1600	Cor + Per
2	90:10	22	1600	Cor + Per
3	90:10	23	1600	Cor + Per + Cf + Gt (tr)
4	90:10	25	1600	Cor + Per + Cf
5	90:10	27	1600	Cf + Cor (tr)
6	78:22	23	1600	Cor + Per + Gt + Cf (tr)
7	78:22	24	1600	Cor + Per + Cf + Gt (tr)
8	78:22	25	1600	Cor + Per + Cf
9	78:22	27	1600	Cf + Cor (tr)
10	70:30	21	1600	Cor + Per + Gt
11	70:30	23	1600	Cor + Per + Gt
12	70:30	24	1600	Cor + Per + Cf + Gt (tr)
13	70:30	27	1600	Cf
14	50:50	23	1600	Cf + Per + Gt + Cor (tr)
15	50:50	24	1600	Cf + Per + Gt
16	50:50	27	1600	Cf + Per + Pv
17	100:0	27	2200	Cf
18	90:10	27	1800	Cf + Cor (tr)
19	70:30	27	1800	Cf + Cor (tr)
20	50:50	27	1800	Cf + Per + Pv

Notes: Duration of all the runs was 3 h except for that of no. 17 (1 h). Cor = corundum, Per = periclase, Cf = calcium ferrite, Gt = garnet, Pv = perovskite, tr = trace amount.

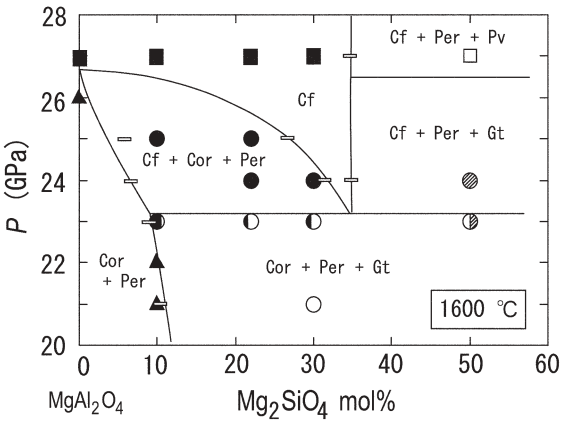

Figure 1. Phase relations in the $MgAl_2O_4$-Mg_2SiO_4 system at 1600 °C. Cf: calcium ferrite, Cor: corundum, Per: periclase, Gt: garnet, Pv: perovskite. Symbols show phase assemblages observed in samples recovered from high-pressure experiments as follows: closed square = Cf; open square = Cf + Per + Pv; closed triangle = Cor + Per; open circle = Cor + Per + Gt; closed circle = Cf + Cor + Per; hatched circle = Cf + Per + Gt. Open square bar represents observed compositional range of Cf or Cor. Two runs of $MgAl_2O_4$ composition are from Akaogi et al. (1999).

TABLE 2. Compositions of phases in the run products

Run no.	1		10		2		3			
Bulk composition	$Sp_{90}Fo_{10}$		$Sp_{70}Fo_{30}$		$Sp_{90}Fo_{10}$		$Sp_{90}Fo_{10}$			
Pressure (GPa)	21		21		22		23			
Phase	Cor	Per	Cor	Gt	Cor	Per	Cor	Gt	Cf	Per
MgO	2.6(5)	98.4(8)	3.9(2)	31.3(9)	3.5(3)	97.5	3.4(3)	32.0(4)	35.8	99.1(12)
Al_2O_3	94.2(9)	1.3(1)	91.5(9)	22.6(7)	91.3(12)	3.8	91.5(9)	23.0(11)	53.0	0
SiO_2	3.4(5)	–	5.5(2)	46.6(12)	5.2(4)	–	5.3(5)	46.3(5)	11.8	–
Total wt%	100.2	99.7	100.9	100.5	100.0	101.3	100.2	101.3	100.6	99.1
Cation number										
Mg	0.07(1)	0.99(1)	0.10(1)	3.13(2)	0.09(1)	0.99	0.09(1)	3.13(2)	1.26	1.00(0)
Al	1.88(2)	0.01(4)	1.81(1)	1.77(3)	1.82(1)	0.01	1.80(2)	1.77(3)	1.46	–
Si	0.06(1)	–	0.09(1)	3.11(2)	0.09(1)	–	0.09(1)	3.11(2)	0.28	–
Total	2.01	1.00	2.00	8.01	2.00	1.00	2.98	8.01	3.00	1.00

Run no.	6		11			14			
Bulk composition	$Sp_{80}Fo_{20}$		$Sp_{70}Fo_{30}$			$Sp_{50}Fo_{50}$			
Pressure (GPa)	23		23			23			
Phase	Gt	Cor	Gt	Cor	Per	Gt	Cor	Cf	Per
MgO	31.8 (8)	4.6(2)	31.7(13)	3.8(3)	97.3(32)	31.5(5)	3.2(9)	35.7(6)	96.0(9)
Al_2O_3	22.9 (10)	87.4(8)	21.5(5)	90.0(9)	0.7(4)	22.0(6)	91.3(17)	52.1(4)	2.2(5)
SiO_2	46.9 (4)	6.8(3)	48.4(18)	5.9(5)	–	47.1(7)	4.2(12)	12.1(4)	–
Total wt%	101.6	98.8	101.6	99.7	98.0	100.6	98.7	99.9	98.2
Cation number									
Mg	3.15 (9)	0.12(1)	3.13(3)	0.10(1)	0.99(1)	3.14(3)	0.08(2)	1.26(2)	0.97(1)
Al	1.78 (7)	1.77(4)	1.67(4)	1.80(1)	0.01(1)	1.73(5)	1.85(4)	1.45(2)	0.02(1)
Si	3.09 (3)	0.12(1)	3.18(1)	0.10(1)	–	3.13(3)	0.07(2)	0.28(1)	–
Total	8.02	2.01	7.98	2.00	1.00	8.00	2.00	2.99	0.99

Run no.	7				12		15		
Bulk composition	$Sp_{80}Fo_{20}$				$Sp_{70}Fo_{30}$		$Sp_{50}Fo_{50}$		
Pressure (GPa)	24				24		24		
Phase	Gt	Cor	Cf	Per	Cor	Cf	Gt	Cf	Per
MgO	31.5(5)	3.0(2)	34.9(3)	96.0(9)	2.9(2)	34.6(3)	30.6(2)	36.9(3)	98.6
Al_2O_3	22.0(6)	91.0(6)	53.1(8)	2.2(5)	90.9(11)	51.9(4)	23.0(4)	48.8(5)	1.9
SiO_2	47.1(7)	4.9(3)	12.7(4)	–	4.5(4)	13.0(3)	45.9(4)	14.3(3)	–
Total wt%	100.6	98.9	100.7	98.2	98.3	99.5	99.5	100.0	100.5
Cation number									
Mg	3.14(3)	0.08(1)	1.22(1)	0.97(1)	0.07(1)	1.22(1)	3.09(2)	1.30(1)	0.98
Al	1.73(5)	1.84(1)	1.46(17)	0.02(1)	1.85(1)	1.44(1)	1.82(3)	1.35(1)	0.01
Si	3.13(3)	0.08(1)	0.30(1)	–	0.08(1)	0.31(1)	3.09(2)	0.34(1)	–
Total	8.00	2.00	2.98	0.99	2.00	2.97	8.00	2.99	0.99

Run no.	4		8		16		
Bulk composition	$Sp_{90}Fo_{10}$		$Sp_{80}Fo_{20}$		$Sp_{50}Fo_{50}$		
Pressure (GPa)	25		25		27		
Phase	Cor	Cf	Cor	Cf	Cf	Pv	Per
MgO	3.0(5)	34.1(3)	2.9(4)	34.1(3)	36.3(4)	38.2(2)	98.2(9)
Al_2O_3	93.3(11)	55.4(5)	93.7(9)	55.3(4)	48.8(8)	6.2(3)	2.0(1)
SiO_2	4.5(7)	11.5(5)	4.3(5)	11.6(5)	14.3(5)	55.3(5)	–
Total wt%	100.8	101.0	100.9	101.0	99.4	99.7	100.2
Cation number							
Mg	0.08(3)	1.19(1)	0.07(1)	1.19(1)	1.29(1)	0.96(1)	0.98(1)
Al	1.85(2)	1.52(2)	1.85(2)	1.51(2)	1.36(2)	0.12(1)	0.01(1)
Si	0.08(1)	0.27(1)	0.07(1)	0.27(1)	0.34(1)	0.93(1)	–
Total	2.01	2.98	1.99	2.97	2.99	2.01	0.99

Notes: Cation numbers of corundum (Cor), periclase (Per), calcium ferrite (Cf), garnet (Gt), and perovskite (Pv) were calculated on the3 O atoms, 1 O atom, 4 O atoms, 12 O atoms, and 3 O atoms bases, respectively. In bulk composition, $Sp_{100-x}Fo_x$ represents (100–x) mol% $MgAl_2O_4$·x mol% Mg_2SiO_4.

mol% $MgSiO_3$. These results suggest that the phase boundary between the assemblages, (corundum + periclase) and (corundum + periclase + garnet), has a large negative slope. Both calcium ferrite phases in run no. 15 at 24 GPa and run no. 16 at 27 GPa have the same averaged composition of $Mg_{1.30}Al_{1.35}Si_{0.34}O_4$. Thus, in Figure 1, there is an almost vertical phase boundary between the fields of calcium ferrite single phase and (calcium ferrite + garnet + periclase) or (calcium ferrite + perovskite + periclase). Furthermore, a "eutectoid" point between the field of calcium ferrite single phase and that of (corundum + periclase + garnet) assemblage is located at about 23 GPa at the composition of 34 mol% Mg_2SiO_4. Both compositions of calcium ferrite and corundum in run no. 7 agree very well with those in run no. 12, both of which were made at 24 GPa. Similarly, at 25 GPa, calcium ferrite and corundum phases of runs no. 4 and no. 8 have consistent compositions. At pressures higher than 23 GPa, the solubility of $MgSiO_3$ component in corundum phase and that of Mg_2SiO_4 in calcium ferrite phase decrease with increasing pressure. Phase boundary curves around the (calcium ferrite + corundum + periclase) assemblage were drawn by combining the compositions of calcium ferrite and corundum phases with the transition pressure of MgO + Al_2O_3 to $MgAl_2O_4$ calcium ferrite at 1600 °C (Akaogi et al. 1999), and the estimated triple point as well as the "eutectoid" point described above. The phase boundary between (calcium ferrite + periclase + garnet) and (calcium ferrite + periclase + perovskite) at 26.5 GPa in Figure 1 was based on the phase relation in $Mg_3Al_2Si_3O_{12}$ determined by Kubo and Akaogi (2000), who used the same high-pressure

apparatus as that in this work.

Most of the periclase grains analyzed in this study included trace amounts of Al component. Since the electron beam in our SEM-EDS analysis irradiated relatively large periclase grains of more than 10 μm in diameter, it is unlikely that the Al component in periclase was due to contamination from neighboring grains of corundum or calcium ferrite. SEM-EDS analysis of garnet grains showed that they have a composition of $Mg_{3.13}Al_{1.74}Si_{3.13}O_3$ within analytical error (Table 2). In the ternary MgO-Al_2O_3-SiO_2 diagram, coexistence of calcium ferrite (or corundum), periclase and garnet is permitted for bulk compositions inside a triangle formed by the compositions of the three phases. Bulk compositions considered in this study are on the join between $MgAl_2O_4$ and Mg_2SiO_4. This join intersects a tie line between MgO (periclase) and $Mg_{3.13}Al_{1.74}Si_{3.13}O_3$ (garnet), one of the three sides of the triangle, at the composition of 22 mol% $MgAl_2O_4$-78 mol% Mg_2SiO_4. This suggests that the stability field of (corundum + periclase + garnet) and (calcium ferrite + periclase + garnet) assemblages may expand to the composition of ~80 mol% Mg_2SiO_4 (Fig. 1).

The composition of perovskite phase is $Mg_{0.96}Si_{0.93}Al_{0.12}O_3$. The amount of magnesium is greater than that of silicon beyond the analytical error. Total cation number is also larger than two although it is within the analytical error. Navrotsky et al. (2003) reported synthesis and properties of nonstoichiometric Al-containing $MgSiO_3$ perovskites with Mg-rich, Si-poor compositions that coexisted with periclase. They concluded that the aluminous perovskites contained oxygen vacancies. As our Mg-rich, Si-poor perovskite coexists with periclase, it is reasonable to assume that the perovskite phase also contains oxygen vacancies. Considering the composition of the perovskite phase, part of the aluminum substitution (about 30%) might be accompanied by occurrence of oxygen vacancies via the mechanism, $2Si^{4+} = 2Al^{3+} + \square_o$ (Navrotsky 1999), while the rest of Al was associated with the Tschermakitic substitution mechanism: $Mg^{2+} + Si^{4+} = 2Al^{3+}$. Similar to the perovskite, some of calcium ferrite solid solutions have a more Si-rich composition than expected from the Tschermakitic substitution. Thus in these phases, the occurrence of cation vacancies on the Mg site might be due to the excess Si^{4+} substitution.

Structural analysis of calcium ferrite-type $MgAl_2O_4$

Figure 2 shows the XRD pattern of calcium ferrite-type $MgAl_2O_4$ analyzed by the Rietveld method, and Table 3 lists the obtained unit-cell parameters, atomic positions and isotropic displacement parameters. The composition of the sample obtained by SEM-EDS is presented in Table 4. There is <1 mol% SiO_2 component in the sample. However, since the amount is small, it was ignored for Rietveld analysis. A few negligibly small peaks of corundum are also seen in the residual in Figure 2. The corundum was probably formed, along with periclase, in the lower temperature region of the sample capsule due to a temperature gradient within it; the peaks of periclase were too weak to be detected. Thus, both corundum and periclase were excluded from the Rietveld refinement. The lattice parameters of calcium ferrite-type $MgAl_2O_4$ were determined to be a = 9.9498(6) Å, b = 8.6468(6) Å, and c = 2.7901(2) Å. In Table 5, these lattice parameters are compared with those reported previously. While our b and c values are in good agreement with previous ones, our a is significantly smaller. The refined atomic positions are very close to those for $CaFe_2O_4$ calcium ferrite (Becker and Kasper 1957). This is not surprising because these two compounds have similar cation radius ratios of $^{VIII}Ca^{2+}/^{VI}Fe^{3+}$ (1.736) and $^{VIII}Mg^{2+}/^{VI}Al^{3+}$ (1.679) (Shannon and Prewitt 1969).

Refined structure is represented in Figure 3. Bond distances and angles in AlO_6 octahedra and in MgO_8 polyhedron are shown in Table 6. Average Al-O distances related to the Al1 and Al2 sites are 1.919 Å and 1.903 Å, respectively. These values are in good agreement with six-coordinated Al-O distances, e.g., 1.929 Å in $NaAlSi_2O_6$ jadeite (Cameron et al. 1973), 1.887 Å in $Mg_3Al_2Si_3O_{12}$ pyrope, 1.924 Å in $Ca_3Al_2Si_3O_{12}$ grossular (Novak and Gibbs 1971), and 1.938 Å in $Y_3Al_5O_{12}$ garnet (Nakatsuka et al. 1999). An O3-Al1-O4' angle of 161.7° indicates that the Al1-O_6 octahedron is significantly deformed. In contrast, Al2-O_6 octahedron is much less deformed. However, Al2 is not at the center of Al2-O_6 octahedron. Rather, it is displaced away from the

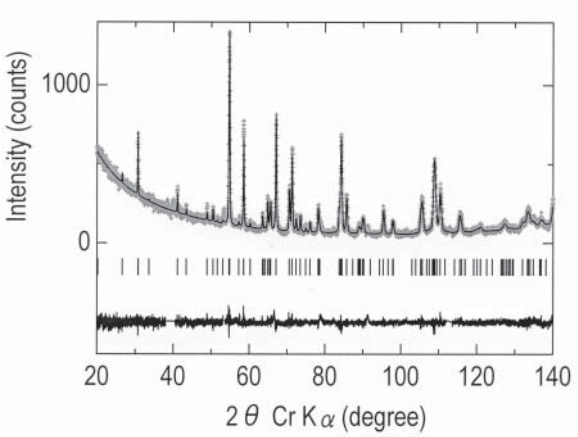

Figure 2. XRD pattern of calcium ferrite-type $MgAl_2O_4$ analyzed by the Rietveld method. Dots and line indicate observed and calculated profiles, respectively. Vertical bars under the profile are peak positions of calcium ferrite-type $MgAl_2O_4$. The plot at the bottom represents the difference between observed and calculated patterns.

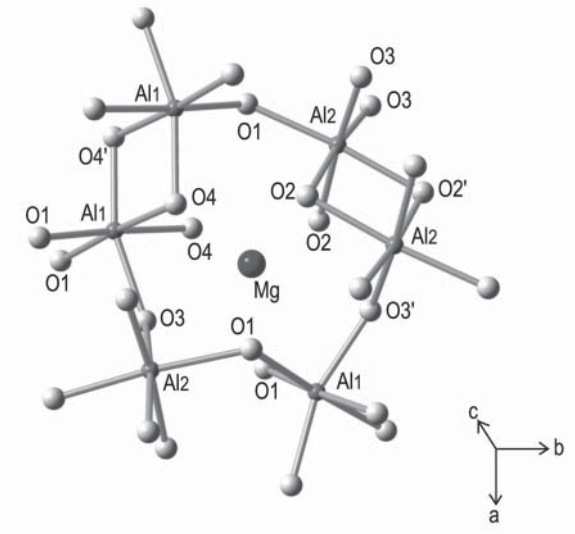

Figure 3. Crystal structure of calcium ferrite-type $MgAl_2O_4$.

TABLE 3. Results of Rietveld refinement of calcium ferrite-type $MgAl_2O_4$

Atom	Site	*x*	*y*	*z*	B_{iso} (Å²)
Mg	4c	0.3503(4)	0.7576(6)	1/4	0.64(13)
Al1	4c	0.3854(4)	0.4388(5)	1/4	0.39(11)
Al2	4c	0.8964(3)	0.4159(4)	1/4	0.30(11)
O1	4c	0.8344(7)	0.2005(8)	1/4	1.59(19)
O2	4c	0.5279(7)	0.1201(6)	1/4	0.84(20)
O3	4c	0.2150(7)	0.5357(8)	1/4	0.88(17)
O4	4c	0.5709(6)	0.4089(7)	1/4	1.57(21)
Space group		*Pbnm*			
a		9.9498(6) Å			
b		8.6468(6) Å			
c		2.7901(2) Å			
V		240.02(2) Å³			
ρ_{calc}		3.937 g/cm³			
R_{WP}, R_B, R_F		9.16%, 5.92%, 3.42%			
χ_w^2		0.91			

Notes: $R_{WP} = \{\Sigma w_i[y_i(o) - y_i(c)]^2/\Sigma w_i[y_i(o)]^2\}^{1/2}$;
$R_B = \Sigma|I_k(o) - I_k(c)|/\Sigma I_k(o)$;
$R_F = \Sigma|[I_k(o)]^{1/2} - [I_k(c)]^{1/2}|/\Sigma[I_k(o)]^{1/2}$;
$\chi_w^2 = \{\Sigma_i[y_i(o) - y_i(c)]^2/\sigma_i^2\}/(n - m)$;
where $y_i(o)$ and $y_i(c)$ are observed and calculated intensities at profile point i, respectively; w_i is a weight for each step i; $I_k(o)$ and $I_k(c)$ are observed and calculated integrated intensities, respectively. n and m in the χ_w^2 calculation show the number of observations and refined parameters, respectively. Isotropic atomic displacement parameter = $\exp[-B_{iso}(\sin\theta/\lambda)^2]$.

TABLE 4. Compositions, lattice parameters, and volumes of calcium ferrite-type $MgAl_2O_4$–Mg_2SiO_4 solid solutions

Run no.	17	18	19	20
Composition (wt%)				
MgO	28.1(5)	31.8(5)	34.3(5)	38.0(5)
Al_2O_3	72.9(6)	62.1(15)	56.2(10)	48.1(10)
SiO_2	0.8(1)	5.9(9)	10.3(5)	15.0(8)
Total	101.8	99.8	100.8	101.1
Cation number				
Mg	0.98(1)	1.13(2)	1.20(1)	1.33(2)
Al	1.99(1)	1.73(4)	1.55(2)	1.32(4)
Si	0.02(1)	0.14(2)	0.24(1)	0.35(2)
Total*	2.99	3.00	2.99	3.00
Lattice parameter (Å)†				
a	9.9498(5)	9.9718(13)	9.9996(8)	10.0176(6)
b	8.6461(5)	8.6403(10)	8.6198(8)	8.6051(5)
c	2.7901(2)	2.7901(3)	2.7921(3)	2.7936(2)
Unit-cell volume (Å³)	240.02(2)	240.39(5)	240.66(5)	240.82(2)
Molar volume (cm³/mol)	36.14(1)	36.19(1)	36.23(1)	36.26(1)
R_{WP} (%)‡	9.16	9.31	10.06	10.58
R_B (%)§	5.92	9.32	8.71	5.30

* Total cation number is calculated on the basis of four O atoms.
† Space group *Pbnm*.
‡ *R* factor of Rietveld analysis on weighted square residual.
§ *R* factor of Rietveld analysis on integrated intensity for calcium ferrite phase.

nearest neighbor Al due to repulsion between these edge-shared octahedra. The nearest Al2-Al2 distance (2.875 Å) is close to that of Al1-Al1 (2.883 Å).

Lattice parameters of $MgAl_2O_4$–Mg_2SiO_4 calcium ferrite solid solutions

Lattice parameters and volumes of calcium ferrite-type $MgAl_2O_4$–Mg_2SiO_4 solid solutions were also determined by Rietveld analysis and are listed in Table 4, together with their compositions. The differences in geometry between the two types of AlO_6 octahedra in the calcium ferrite-type $MgAl_2O_4$ suggest that Si^{4+} might prefer the Al2 site because of its more symmetric shape and slightly smaller size compared with Al1. To test this hypothesis, XRD data for 66 mol% $MgAl_2O_4$-34 mol% Mg_2SiO_4 phase were analyzed using different schemes of Al/Si distribution. Our results show that a random Al/Si distribution gives the lowest R_B factor, 5.3%, compared with 6.0% and 5.9% for the preferred distribution of Si^{4+} in Al1 and Al2 sites, respectively. Thus, it is more probable that Mg^{2+} and Si^{4+} randomly substitute for Al^{3+} in both the Al1 and Al2 sites.

TABLE 5. Comparison of lattice parameters of calcium ferrite-type $MgAl_2O_4$ at 1 atm

	a (Å)	*b* (Å)	*c* (Å)	*V* (Å³)
This study	9.9498(6)	8.6468(6)	2.7901(2)	240.02(2)
Irifune et al. (1991)	9.969(3)	8.631(3)	2.789(1)	240.0(2)
Yutani et al. (1997)	9.966(3)	8.634(3)	2.789(1)	240.0(2)
Funamori et al. (1998)	9.977(4)	8.649(3)	2.785(1)	240.3(2)

TABLE 6. Atomic distances and bond angles for calcium ferrite-type $MgAl_2O_4$

	Distance (Å)	O-M-O angle (°)
AlO_6 octahedra		
Al1-O1 ×2	1.912(6)	
Al1-O3	1.891(7)	
Al1-O4 ×2	1.967(6)	
Al1-O4′	1.864(7)	
average	1.919	
O1-O1	2.790(1)	93.7(4)
O1-O4 ×2	2.691(9)	87.9(2)
O4-O4	2.790(1)	90.3(3)
O3-O1 ×2	2.744(9)	92.4(3)
O3-O4 ×2	2.591(5)	84.4(3)
O4′-O1 ×2	2.894(8)	100.1(3)
O4′-O4 ×2	2.533(8)	82.7(3)
Al2-O1	1.962(8)	
Al2-O2 ×2	1.938(6)	
Al2-O2′	1.919(7)	
Al2-O3 ×2	1.830(5)	
average	1.903	
O2-O2	2.790(1)	92.1(3)
O2-O3 ×2	2.524(10)	84.1(2)
O3-O3	2.790(1)	99.3(4)
O1-O2 ×2	2.839(9)	93.4(2)
O1-O3 ×2	2.719(8)	91.5(3)
O2′-O2 ×2	2.563(10)	83.3(2)
O2′-O3 ×2	2.688(8)	91.6(3)
MgO_8 polyhedron		
Mg-O1 ×2	2.336(7)	
Mg-O2 ×2	2.129(6)	
Mg-O3	2.344(10)	
Mg-O3′	2.491(10)	
Mg-O4 ×2	2.152(6)	
average	2.259	

Raman spectra of pure calcium ferrite-type $MgAl_2O_4$ and calcium ferrite solid solutions, 73 and 66 mol% $MgAl_2O_4$, are shown in Table 7 and Figure 4. According to McMillan et al. (1989), peak broadening is generally associated with structural disorder over lattice sites, i.e., Mg, Si, and Al disorder over the octahedral site in the pyrope-majorite garnet solid solutions. The strongest Raman line of the calcium ferrite-type $MgAl_2O_4$ at 707 cm^{-1} has been assigned to the stretching mode of AlO_6 octahedra (Kojitani et al. 2003). Both the calcium ferrite-type $MgAl_2O_4$–Mg_2SiO_4 solid solutions with the $MgAl_2O_4$ content of 73 and 66 mol% have the Raman line much broader than that of pure calcium ferrite-type $MgAl_2O_4$. This supports the argument of disorder of Mg^{2+}, Si^{4+}, and Al^{3+} over both the Al1 and Al2 sites and is consistent with the smallest R_B for Rietveld refinement based on the disordered distribution. Hence, the random distribution model was adopted in the refinements for all the composition.

The lattice parameters are listed in Table 4. The lattice parameter-composition relations are plotted in Figure 5. The *a* and *c* parameters increase with increasing Mg_2SiO_4 component,

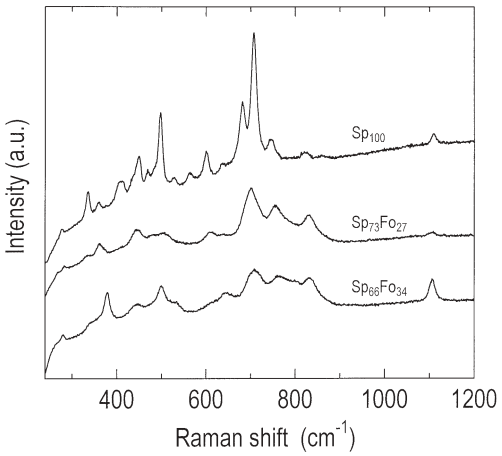

FIGURE 4. Raman spectra of calcium ferrite-type $MgAl_2O_4$–Mg_2SiO_4 solid solutions. Sp and Fo represent $MgAl_2O_4$ and Mg_2SiO_4 component (mol%), respectively.

TABLE 7. Observed Raman shifts and peak widths of calcium ferrite-type $MgAl_2O_4$–Mg_2SiO_4 solid solutions

$MgAl_2O_4$		$MgAl_2O_4$:Mg_2SiO_4 = 73:27		$MgAl_2O_4$:Mg_2SiO_4 = 66:34	
Raman shift (cm^{-1})	FWHM (cm^{-1})	Raman shift (cm^{-1})	FWHM (cm^{-1})	Raman shift (cm^{-1})	FWHM (cm^{-1})
240	6				
277	7	283	8	279	10
317	10				
329	5				
336	9	333	19	341	22
				360	21
359	10	361	19	378	15
403	14				
413	12				
435	14				
449	14	445	29	445	33
469	11	478	25	472	18
483	14				
498	11	505	40	500	29
528	13			532	22
564	13				
600	13	613	28	612	26
637	13	641	25	647	39
661	32			673	24
681	16	696	25	700	31
707	15	707	41	718	37
747	26	760	39	767	51
		792	33	800	30
821	19	834	41	836	45
1109	13	1106	19	1106	16

Note: FWHM = Full width at half maximum.

although c increases at a much lower rate than a. On the other hand, b decreases with increasing Mg_2SiO_4. A linear regression of lattice parameters vs. composition yields the following relations:

$$a = 9.9498 + 0.1947 \cdot X_{Mg_2SiO_4} \quad (1)$$

$$b = 8.6468 - 0.1097 \cdot X_{Mg_2SiO_4} \quad (2)$$

$$c = 2.7901 + 0.0086 \cdot X_{Mg_2SiO_4} \quad (3)$$

where a, b, and c are in Å and $X_{Mg_2SiO_4}$ is the mole fraction of Mg_2SiO_4 component in calcium ferrite solid solution. The correlation factors (|r|) of Equations 1, 2, and 3 are 0.988, 0.944, and 0.804, respectively. With increasing Mg_2SiO_4 component, unit-cell volume increases approximately linearly (Fig. 5). A linear

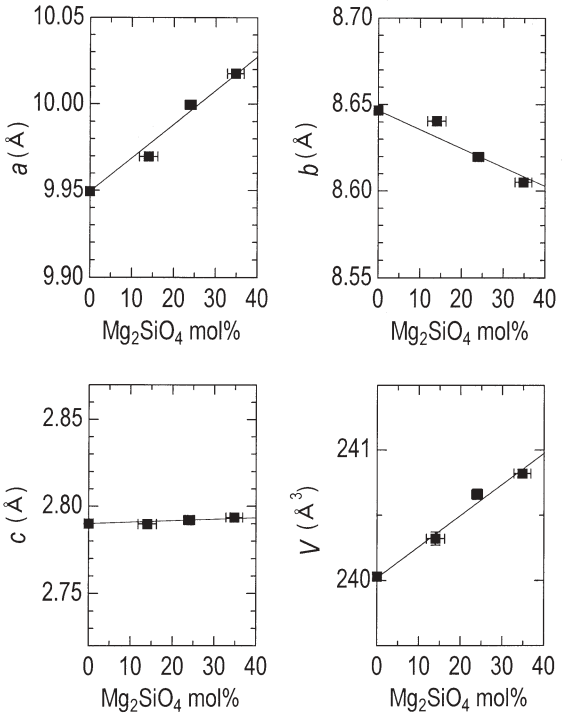

FIGURE 5. Lattice parameters and unit-cell volumes of the calcium ferrite-type $MgAl_2O_4$–Mg_2SiO_4 solid solutions. Solid lines show fitted lines by the least-squares method.

fitting of the volume data gives the following equation:

$$V = 240.02 + 2.403 \cdot X_{Mg_2SiO_4} \quad (4)$$

where V is in $Å^3$. According to Shannon and Prewitt (1969), the six coordinated ionic radii of Mg^{2+}, Al^{3+}, and Si^{4+} are 0.72, 0.53, and 0.40 Å, respectively. The replacement of Mg^{2+} for Al^{3+} may expand the size of AlO_6 octahedra while the substitution of Si^{4+} for Al^{3+} may contract it. Since the difference in the ionic radius between Mg^{2+} and Al^{3+} is larger than that between Al^{3+} and Si^{4+}, the average size of AlO_6, MgO_6, and SiO_6 octahedra is expected to be larger than those in the pure calcium ferrite-type $MgAl_2O_4$ if they are randomly distributed. If the coupled substitution of Mg^{2+} and Si^{4+} for Al^{3+} provides, on average, larger AlO_6 octahedra, the unit-cell volume will become larger. This is consistent with the results in Figure 5.

Variations of molar volume as a function of composition are plotted in Figure 6. As noted above, the relationship between composition and volume is linear within the errors. By extrapolating the fitted line to the Mg_2SiO_4 end-member, the molar volume and density (ρ_{calc}) of the hypothetical Mg_2SiO_4 calcium ferrite are estimated to be 36.49(2) cm^3/mol and 3.856(2) g/cm^3, respectively. The zero-pressure density is lower than that estimated by Liu (1977) (3.93 g/cm^3). The results of the distance least squares (DLS) calculation by Yamada et al. (1983) gave a volume of 37.26 cm^3/mol, which is considerably larger than our value.

The summation of volumes of $MgSiO_3$ perovskite (Dobson and Jacobsen 2004) and MgO (Tsirelson et al. 1998) is 35.72(1) cm^3/mol. The volume of the hypothetical calcium ferrite-type

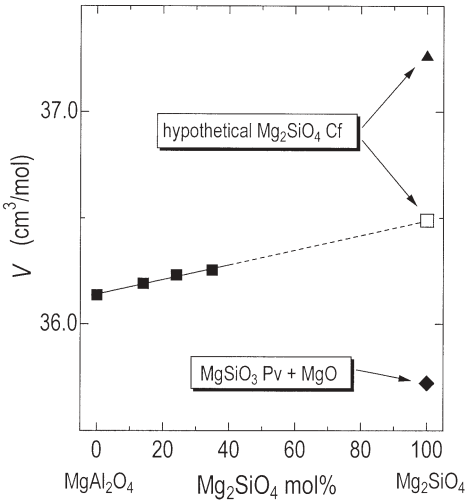

FIGURE 6. Estimation of molar volume for the hypothetical calcium ferrite-type Mg_2SiO_4. Solid squares represent observed molar volumes of calcium ferrite-type $MgAl_2O_4$–Mg_2SiO_4 solid solutions. The open square represents molar volume of the hypothetical calcium ferrite-type Mg_2SiO_4 estimated by extrapolation of the data in this study. A solid line shows linear regression of the observed volumes. Dashed line shows a linear extrapolation of the regression line. Solid triangle shows an estimated volume using distance least squares calculation by Yamada et al. (1983). Solid diamond is the summation of volume of $MgSiO_3$ perovskite (Dobson and Jacobsen 2004) and that of MgO (Tsirelson et al. 1998).

Mg_2SiO_4 from this study is about 0.8 cm^3/mol larger than that of the isochemical mixture of $MgSiO_3$ perovskite and MgO. This difference suggests that ($MgSiO_3$ perovskite + MgO) is more preferred energetically than calcium ferrite-type Mg_2SiO_4 at high pressure. This is consistent with the fact that synthesis of calcium ferrite-type Mg_2SiO_4 has never been reported.

$NaAlSiO_4$ is a major component of the phase with the calcium ferrite structure in the high-pressure phase assemblage of MORB (e.g., Guignot and Andrault 2004). Because the hypothetical calcium ferrite-type Mg_2SiO_4 has a larger molar volume and a smaller formula weight than those of calcium ferrite-type $NaAlSiO_4$, it is suggested that increase in solubility of Mg_2SiO_4 component decreases the density of the calcium ferrite phase in MORB.

ACKNOWLEDGMENTS

We thank A. Kubo for useful advices for synthesizing $MgAl_2O_4$ calcium ferrite, M. Ozima for providing $MgSiO_3$ orthoenstatite used as a standard in SEM-DES analysis, and J.M. Neil for proofreading. We are also grateful to H. Xu for helpful comments. This work was supported in part by Grants-in-Aid for Scientific Research, (C) 18540478 to H. Kojitani and (A) 15204049 to M. Akaogi, from the Japan Society for the Promotion of Science.

REFERENCES CITED

Akaogi, M., Hamada, Y., Suzuki, T., Kobayashi, M., and Okada, M. (1999) High pressure transitions in the system $MgAl_2O_4$–$CaAl_2O_4$: a new hexagonal aluminous phase with implication for the lower mantle. Physics of the Earth and Planetary Interiors, 115, 67–77.

Becker, D.F. and Kasper, J.S. (1957) The structure of calcium ferrite. Acta Crystallographica, 10, 332–337.

Cameron, M., Sueno, S., Prewitt, C.T., and Papike, J.J. (1973) High-temperature crystal chemistry of acmite, diposide, hedenbergite, jadeite, spodumene, and ureyite. American Mineralogist, 58, 594–618.

Dobson, D.P. and Jacobsen, S.D. (2004) The flux growth of magnesium silicate perovskite single crystals. American Mineralogist, 89, 807–811.

Funamori, N., Jeanloz, R., Nguyen, J.H., Kavner, A., and Caldwell, W.A. (1998) High-pressure transformations in $MgAl_2O_4$. Journal of Geophysical Research, 103, 20813–20818.

Funamori, N., Jeanloz, R., Miyajima, N., and Fujino, K. (2000) Mineral assemblages of basalt in the lower mantle. Journal of Geophysical Research, 105, 26037–26043.

Guignot, N. and Andrault, D. (2004) Equations of state of Na-K-Al host phases and implications for MORB density in the lower mantle. Physics of the Earth and Planetary Interiors, 143–144, 107–128.

Hirose, K., Fei, Y., Ma, Y., and Mao, H.K. (1999) The fate of subducted basaltic crust in the Earth's lower mantle. Nature, 397, 53–56.

Irifune, T., Fujino, K., and Ohtani, E. (1991) A new high-pressure form of $MgAl_2O_4$. Nature, 349, 409–411.

Irifune, T., Naka, H., Sanehira, T., Inoue, T., and Funakoshi, K. (2002) In situ X-ray observations of phase transitions in $MgAl_2O_4$ spinel to 40 GPa using multianvil apparatus with sintered diamond anvils. Physics and Chemistry of Minerals, 29, 645–654.

Ito, E. and Takahashi, E. (1989) Postspinel transitions in the system Mg_2SiO_4-Fe_2SiO_4 and some geophysical implications. Journal of Geophysical Research, 94, 10637–10646.

Izumi, F. and Ikeda, T. (2000) A Rietveld-analysis program RIETAN-98 and its applications to zeolites. Materials Science Forum, 321–324, 198–204.

Kesson, S.E., Fitz Gerald, J.D., and Shelley, J.M.G. (1994) Mineral chemistry and density of subducted basaltic crust at lower-mantle pressures. Nature, 372, 767–769.

Kojitani, H., Nishimura, K., Kubo, A., Sakashita, M., Aoki, K., and Akaogi, M. (2003) Raman spectroscopy and heat capacity measurement of calcium ferrite type $MgAl_2O_4$ and $CaAl_2O_4$. Physics and Chemistry of Minerals, 30, 409–415.

Kubo, A. and Akaogi, M. (2000) Post-garnet transitions in the system $Mg_4Si_4O_{12}$-$Mg_3Al_2Si_3O_{12}$ up to 28 GPa: phase relations of garnet, ilmenite and perovskite. Physics of the Earth and Planetary Interiors, 121, 85–102.

Liu, L. (1977) High pressure $NaAlSiO_4$: the first silicate calcium ferrite isotype. Geophysical Research Letters, 4, 183–186.

McMillan, P., Akaogi, M., Ohtani, E., Williams, Q., Nieman, R., and Sato, R. (1989) Cation disorder in garnets along the $Mg_3Al_2Si_3O_{12}$–$Mg_4Si_4O_{12}$ join: an infrared, Raman and NMR study. Physics and Chemistry of Minerals, 16, 428–435.

Morishima, H., Kato, T., Suto, M., Ohtani, E., Urakawa, S., Utsumi, W., Shimomura, O., and Kikegawa, T. (1994) The phase boundary between α- and β-Mg_2SiO_4 determined by in situ X-ray observation. Science, 265, 1202–1203.

Nakatsuka, A., Yoshiasa, A., and Yamanaka, T. (1999) Cation distribution and crystal chemistry of $Y_3Al_{5-x}Ga_xO_{12}$ ($0 \le x \le 5$) garnet solid solutions. Acta Crystallographica, B55, 266–272.

Navrotsky, A. (1999) A lesson from ceramics. Science, 284, 1788–1789.

Navrotsky, A., Schoenitz, M., Kojitani, H., Xu, H., Zhang, J., Weidner, D.J., and Jeanloz, R. (2003) Aluminum in magnesium silicate perovskite: Formation, structure, and energetics of magnesium-rich defect solid solutions. Journal of Geophysical Research, 108 (B7), 2330, DOI: 10.1029/2002JB002055.

Novak, G.A. and Gibbs, G.V. (1971) The crystal chemistry of the silicate garnets. American Mineralogist, 56, 791–823.

Ono, S., Ito, E., and Katsura, T. (2001a) Mineralogy of subducted basaltic crust (MORB) from 25 to 37 GPa, and chemical heterogeneity of the lower mantle. Earth and Planetary Science Letters, 190, 57–63.

Ono, S., Katsura, T., Ito, E., Kanzaki, M., Yoneda, A., Walter, M.J., Urakawa, S., Utsumi, W., and Funakoshi, K. (2001b) In situ observation of ilmenite-perovskite phase transition in $MgSiO_3$ using synchrotron radiation. Geophysical Research Letters, 28, 835–838.

Ono, S., Hirose, K., Kikegawa, T., and Saito, Y. (2002) The compressibility of a natural composition calcium ferrite-type aluminous phase to 70 GPa. Physics of the Earth and Planetary Interiors, 131, 311–318.

Ringwood, A.E., Reid, A.F., and Wadsley, A.D. (1967) High pressure transformation of alkali aluminosilicates and aluminogermanates. Earth and Planetary Science Letters, 3, 38–40.

Shannon, R.D. and Prewitt, C.T. (1969) Effective ionic radii in oxides and fluorides. Acta Crystallographica, B25, 925–946.

Suzuki, T. and Akaogi, M. (1995) Element partitioning between olivine and silicate melt under high pressure. Physics and Chemistry of Minerals, 22, 411–418.

Tsirelson, V.G., Avilov, A.S., Abramov, Y.A., Belokoneva, E.L., Kitaneh, R., and Feil, D. (1998) X-ray and electron diffraction study of MgO. Acta Crystallographica, B54, 8–17.

Yamada, H., Matsui, Y., and Ito, E. (1983) Crystal-chemical characterization of $NaAlSiO_4$ with the $CaFe_2O_4$ structure. Mineralogical Magazine, 47, 177–181.

Yutani, M., Yagi, T., Yusa, H., and Irifune, T. (1997) Compressibility of calcium ferrite-type $MgAl_2O_4$. Physics and Chemistry of Minerals, 24, 340–344.

MANUSCRIPT RECEIVED MARCH 3, 2006
MANUSCRIPT ACCEPTED JANUARY 31, 2007
MANUSCRIPT HANDLED BY HONGWU XU